Scientific Research Publishing

Journal of Power and Energy Engineering, 2020, 8, 65-93
https://www.scirp.org/journal/jpee
ISSN Online: 2327-5901
ISSN Print: 2327-588X

A Simplified Simulation Procedure and Analysis of a Photovoltaic Solar System Using a Single Diode Model

Robinson Ndegwa, Elijah Ayieta, Justus Simiyu, Nicodemus Odero

Department of Physics, University of Nairobi, Nairobi, Kenya
Email: ndegwarg@uonbi.ac.ke

How to cite this paper: Ndegwa, R., Ayieta, E., Simiyu, J. and Odero, N. (2020) A Simplified Simulation Procedure and Analysis of a Photovoltaic Solar System Using a Single Diode Model. *Journal of Power and Energy Engineering*, **8**, 65-93.
https://doi.org/10.4236/jpee.2020.89006

Received: August 28, 2020
Accepted: September 26, 2020
Published: September 29, 2020

Abstract

A single diode model for a photovoltaic solar module is the most ideal and quick way of analyzing the module characteristics before implementing them in a solar plant. Solar modules manufacturers provide information for three critical points that are essential in I-V, P-V or P-I curves. In this study, we propose four separate simulation procedures to estimate the five-model parameters of an analogous single diode equivalent circuit by utilizing three cardinal points of the photovoltaic module I-V curve, described from experimental data using a solar simulator and manufacturer's datasheet. The main objective is to extract and use the five unknown parameters of a single diode model to describe the photovoltaic system using I-V ad P-V plots under different environmental conditions. The most influential parameters that greatly alter the cardinal points defined at short circuit point (SCP), the maximum power point (MPP) and the open circuit point(OCP) are the ideality factor (n) and the diode saturation current (I_o). For a quick and fast convergence, we have determined the optimal ideality factor (n_o) and optimal saturation current (I_{oopt}) as the primary parameters by first assuming the optimal values of R_{sh}, R_s and I_{ph} at standard test conditions (STC). Further, we evaluated the effects of I_{ph}, R_s and R_{sh} on I-V and P-V curves by considering the values of n below n_o. We have evaluated different iterative procedures of determining R_{sh} and R_s at open-circuit, short-circuit point and the maximum-power points. These procedures have been classified into four approaches that guarantees positive shunt and series resistance for $n \leq n_o$. These approaches have been categorized by deriving the saturation current as a dependent variable at each cardinal point with or without R_s and R_{sh} pair. The values obtained for the five parameters have been used to simulate the photovoltaic solar module characteristic curves with great precision at different air temperatures and irradiances, considering the effect of Nominal Operating Cell Temperature

(NOCT).

Keywords

Five-Parameter Model, Ideality Factor, Saturation Current, Series and Shunt Resistances

1. Introduction

Harvesting of renewable solar energy has grown rapidly over the past decade due to the availability of cheap and affordable modules and deep-cycle energy storage systems [1]. Although the installation of solar photovoltaic systems faces different challenges, the solar power has the highest potential in the world as a major source of clean energy [2] [3]. Some of these challenges include diverse environmental factors such as varying solar irradiance and temperatures, dust and shades, low solar cell efficiency and high installation costs [4]. These drawbacks have attracted numerous research works for tracking the optimum power generated by a photovoltaic module at various environmental conditions in order to improve its efficiency [5]-[10]. Photovoltaic systems should be optimized to work at the maximum power for any solar irradiation level and ambient temperature. Modeling and simulation of the photovoltaic systems gives a better understanding of the maximum power point using characteristic curves [11].

A single diode model of a solar system has been studied for decades since it offers an elaborate, simple and reliable analysis of the current-voltage characteristics of solar cells [12] [13] [14]. The model requires extremely thorough and careful computation of I_{ph}, I_o, n, R_s and R_{sh} parameters that are based on the equivalent circuit analysis using Schottky's diode equation [15].

Several techniques based on soft computing have been studied for unknown parameters determination using evolutionary algorithms [16]. These methods are strongly convergent and have less computing time. However, due to their stochastic nature, their efficiency depends on the choice of control parameters and search ranges which require high computational power [17] [18].

Analytical and numerical methods are the traditional techniques for estimating all parameters of a single diode photovoltaic model [19] [20]. The analytical approach relies heavily on the availability of data for short-circuit current (I_{sc}), maximum power point voltage (V_{mpp}), maximum power point current (I_{mpp}), open-circuit voltage (V_{oc}) and IV-curve intersection slopes [21] [22] [23]. Several authors have used information provided from the manufacturer's datasheets for I_{sc}, V_{oc}, I_{mpp}, V_{mpp} to determine the photovoltaic parameters *using nonlinear* least square (NLS) algorithm [24], normalized root mean-square deviation (NRMSD) [25] [26], Newton-Raphson algorithm [27] [28] and Lambert W Function [29] [30] [31] [32] [33]. These approaches offer quick, robust and faster ways of extracting the parameters of a single-diode photovoltaic model. The precision of these approaches is based primarily on the accuracy of the data pro-

vided for the three crucial points on the I-V curve [20]. Standard photovoltaic module datasheet values for I_{sc}, V_{oc}, I_{mpp} and V_{mpp} are approximated to one or two decimal places while P_{mpp} values are given in the nearest tenth for all modules with the same power rating. However, each solar module has its individual values for each of these points at STC [34]. Therefore datasheet values can introduce significant errors in simulating the I-V or P-V curves. Numerical methods, on the contrary, are based on iterative algorithms for fitting simulated I-V curves into the experimental data [20] [35] [36]. This paper presents combined analytical and numerical approaches for determining the ideality factor (n), diode saturation current (I_o), photocurrent (I_{ph}), series (R_s) and shunt (R_{sh}) resistances for a single diode photovoltaic model. The analytical approach gives a straightforward, simple and rapid way of extracting ideality factor and saturation current by approximating their optimum values using three critical points from either the data sheet and/or the experimental data. The numerical approach gives the precise values of the ideality factor and saturation current in the proximity of optimal ideality factor (n_o) and optimal saturation current (I_{opt}) respectively. Further, series (R_s) and shunt (R_{sh}) resistances that are not provided in the manufacturer's datasheet are determined using iterative algorithms. Finally, the photo current is explicitly determined using the extracted n, I_o, R_s, R_{sh} and datasheet or experimental values. A comparison of simulated I-V and P-V curves from datasheet and experimental data values is also presented for different environmental conditions.

2. A Single Diode Model

Figure 1 shows a single diode equivalent circuit that can be evaluated using Equation (1). A current source is connected in series to R_s and in parallel to the Shockley's diode [37] and shunt resistor R_{sh}.

The equivalent circuit can be presented mathematically by

$$I = I_{ph} - I_o\left(\exp\left(\frac{q\left(V + IR_s\right)}{nKT}\right) - 1\right) - \frac{V + IR_s}{R_{sh}}. \quad (1)$$

where; T = 298.15 K, q is the charge of an electron = $1.602176634 \times 10^{-19}$ C and k is the Boltzmann's Constant = 1.380649×10^{-23} $m^2 \cdot s^{-2} \cdot kg \cdot K^{-1}$.

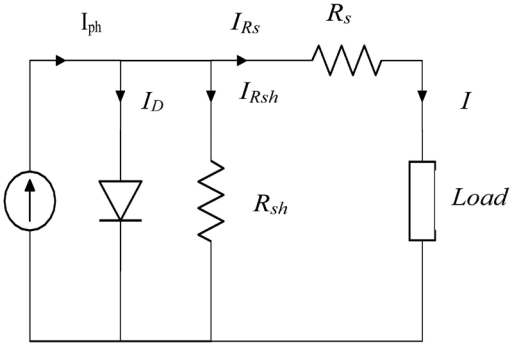

Figure 1. A single diode equivalent circuit.

3. Evaluation of a Single Diode Model at Three Critical Points in I-V and P-V Curves

The critical points of I-V and P-V curves for a photovoltaic system are the short circuit (SC), the maximum power point (MPP) and open-circuit (OC). These points play an important role since a quick look at their values gives a clear picture of the photovoltaic module characteristic and performance. We can use Equation (1) and rearrange it at each point as follows:

1) At short circuit, $I = I_{sc}$, $V = 0$;

We can rewrite Equation (1) as

$$I_{sc} = I_{ph} - I_o\left(\exp\frac{I_{sc}R_s}{nN_sV_t} - 1\right) - \frac{I_{sc}R_s}{R_{sh}}. \tag{2}$$

or

$$I_{ph} = I_{sc} + I_o\left(\exp\frac{I_{sc}R_s}{nN_sV_t} - 1\right) + \frac{I_{sc}R_s}{R_{sh}}. \tag{3}$$

where $V_t = kT/q = 0.025692607$ is the thermal voltage.

2) At Open Circuit, $I = 0$, $V = V_{oc}$;

Equation (1) can be rearranged as

$$I_{ph} = I_o\left(\exp\frac{V_{oc}}{nN_sV_t} - 1\right) + \frac{V_{oc}}{R_{sh}}. \tag{4}$$

3) At Maximum Power Point, $I = I_{mpp}$, $V = V_{mpp}$;

We can similarly replace $I = I_{mpp}$, $V = V_{mpp}$ in equation to obtain

$$I_{mpp} = I_{ph} - I_o\left(\exp\frac{V_{mpp} + I_{mpp}R_s}{nN_sV_t} - 1\right) - \frac{V_{mpp} + I_{mpp}R_s}{R_{sh}}. \tag{5}$$

The above equations can be used to evaluate and determine the five unknown parameters using the experimental or manufacturer's data as discussed in the following sections.

4. Determination of Unknown Parameters for a Single Diode Photovoltaic Model

The transcendental Equation (1) has five unknown parameters that must be determined in order to have a model that represents the experimental data. These parameters include photocurrent (I_{ph}), ideality factor (n), saturation current (I_o), series (R_s) and shunt (R_{sh}) resistances that can be derived using I_{sc}, I_{mpp}, V_{oc} and V_{mpp}.

The following sections 4.1 to 4.3, addresses a detailed mathematical derivation of I_{ph}, I_o and n equations, outlining the disadvantages and benefits of each method. Section 4.4 discusses analytical approaches for R_s and R_{sh} determination.

4.1. Photocurrent (I_{ph}) Analysis

The photocurrent (I_{ph}) can be determined from Equations ((2), (3)) or by re-

writing Equation (5) as

$$I_{ph} = I_{mpp} + I_o\left(\exp\frac{V_{mpp} + I_{mpp}R_s}{nN_sV_t} - 1\right) + \frac{V_{mpp} + I_{mpp}R_s}{R_{sh}}. \quad (6)$$

However, I_{ph} depends on the solar irradiance and module surface temperature (T). Therefore, the relationship between I_{ph}, T and actual irradiance (s_a) can be deduced using temperature coefficient of short circuit current (K_I) as discussed in [27] [38] [39]. Thus,

$$I_{ph} = \frac{s_a}{s_{STC}}\left[I_{ph_{STC}} + K_I\left(T - T_{STC}\right)\right]. \quad (7)$$

4.2. Saturation Current (I_o)

The saturation current can be evaluated using Equation (1) at the three critical points by maintaining constant temperature at the standard test condition, where $T_{STC} = 25^{\circ}\text{C}$.

4.2.1. Saturation Current (I_o) at Each Critical Point

1) At the short circuit, Equation (2) can be rearranged to give

$$I_o = \frac{I_{ph}R_{sh} - I_{sc}R_{sh} - I_{sc}R_s}{R_{sh}\left(\exp\left(\frac{I_{sc}R_s}{nN_sV_t}\right) - 1\right)}. \quad (8)$$

2) At maximum power point, Equation (5) can be reorganized to obtain

$$I_o = \frac{I_{ph}R_{sh} - I_{mpp}R_{sh} - V_{mpp} - I_{mpp}R_s}{R_{sh}\left(\exp\left(\frac{V_{mpp} + I_{mpp}R_s}{nN_sV_t}\right) - 1\right)}. \quad (9)$$

Setting the boundary condition of $R_s \approx 0$, $R_{sh} \approx \infty$ and $I_{ph} \approx I_{sc}$, Equation (9) yields

$$I_o = \frac{I_{sc} - I_{mpp}}{\exp\frac{V_{mpp}}{nN_sV_t} - 1}. \quad (10)$$

3) At the open circuit, Equation (4) can be rearranged to give

$$I_o = \frac{I_{ph}R_{sh} - V_{oc}}{R_{sh}\left(\exp\left(\frac{V_{oc}}{nN_sV_t}\right) - 1\right)}. \quad (11)$$

Similarly, setting boundary condition of $R_{sh} \approx \infty$ and $I_{ph} \approx I_{sc}$, Equation (11) yields

$$I_o = \frac{I_{sc}}{\exp\left(\frac{V_{oc}}{nN_sV_t}\right) - 1}. \quad (12)$$

4.2.2. Saturation Current (I_o) Calculation by Combining Two Out of Three Critical Point Equations

The saturation current can also be calculated by combining two of either Equations ((3), (4) or (6)). Subtracting Equations ((3) and (4)) eliminates I_{ph} as re-

ported by [27] [40] and [41]. This reduces to

$$\left[I_o\right]_{I_{sc},V_{oc}} = \frac{I_{sc}R_{sh} + I_{sc}R_s - V_{oc}}{R_{sh}\left(\exp\left(\frac{V_{oc}}{nN_sV_t}\right) - \exp\left(\frac{I_{sc}R_s}{nN_sV_t}\right)\right)}. \tag{13}$$

Once more, taking $R_s \approx 0$ and $R_{sh} \approx \infty$, we can rewrite Equation (13) as

$$\left[I_{o_{opt}}\right]_{I_{sc},V_{oc}} = \frac{I_{sc}}{\exp\left(\frac{V_{oc}}{nN_sV_t}\right)}. \tag{14}$$

Similarly, Equation (3) can be merged with Equation (6) at I_{sc} and P_{mpp} to obtain

$$\left[I_o\right]_{I_{sc},P_{mpp}} = \frac{V_{mpp} + I_{mpp}R_{sh} + I_{mpp}R_s - I_{sc}R_s - I_{sc}R_{sh}}{R_{sh}\left(\exp\left(\frac{I_{sc}R_s}{nN_sV_t}\right) - \exp\left(\frac{V_{mpp} + I_{mpp}R_s}{nN_sV_t}\right)\right)}. \tag{15}$$

Returning to $R_s \approx 0$ and $R_{sh} \approx \infty$, Equation (15) reduces to

$$\left[I_{o_{opt}}\right]_{I_{sc},P_{mpp}} = \frac{I_{sc} - I_{mpp}}{\exp\left(\frac{V_{mpp}}{nN_sV_t}\right)}. \tag{16}$$

Finally, considering Equations ((4) and (6)) at V_{oc} and P_{mpp}, we can deduce the saturation current as

$$\left[I_o\right]_{V_{oc},P_{mpp}} = \frac{V_{mpp} - V_{oc} + I_{mpp}R_{sh} + I_{mpp}R_s}{R_{sh}\left(\exp\left(\frac{V_{oc}}{nN_sV_t}\right) - \exp\left(\frac{V_{mpp} + I_{mpp}R_s}{nN_sV_t}\right)\right)}. \tag{17}$$

Again, assuming $R_s \approx 0$ and $R_{sh} \approx \infty$, we can rewrite Equation (17) as

$$\left[I_{o_{opt}}\right]_{V_{oc},P_{mpp}} = \frac{I_{mpp}}{\exp\left(\frac{V_{oc}}{nN_sV_t}\right) - \exp\left(\frac{V_{mpp}}{nN_sV_t}\right)}. \tag{18}$$

4.2.3. Dependence of the Saturation Current on Temperature

The dark saturation current has been reported to be independent of irradiance and has been regarded as the reverse saturation current which is the reverse current in a solar cell caused by diffusion of minority carriers from the neutral regions to the depletion region in the absence of irradiation [42] [43]. However, the dark saturation current strongly depends on the parameters of the temperature, the cross-sectional area of semiconductor and the concentration of the intrinsic carrier [43] [44]. The intrinsic carrier concentration number also depends on the state conduction and valence band densities and the semiconductor energy band-gap (E_g) [44]. Therefore, as discussed by [45] [46], saturation current density can be derived as

$$J_o = qAN_VN_C\left[\frac{1}{N_A}\sqrt{\frac{D_{n-}}{\tau_{n-}}} + \frac{1}{N_D}\sqrt{\frac{D_{p+}}{\tau_{p+}}}\right]\exp\left(\frac{-E_g}{kT}\right). \tag{19}$$

where N_V, is the effective density of states in the valence band, N_C is the effective density of states in the conduction band, N_A is acceptor impurities concentration, N_D is donor impurities concentration, τ_{n-} is electron (minority carrier) lifetime, τ_{p+} is hole (minority carrier) lifetime, A is cross-sectional area of solar cell, E_g is the energy band-gap, D_{n-} is electron diffusion coefficient and D_{p+} is hole diffusion coefficient.

Applying Equation (1) to a solar module as explained by [47], we can obtain

$$I_o = I_{o_{STC}} \left[\frac{T}{T_{STC}}\right]^3 \exp\frac{-qE_g}{nN_s}\left(\frac{1}{T_{STC}} - \frac{1}{T}\right). \tag{20}$$

The saturation current can be calculated using Equations (8) to (18) at constant temperature of 25˚C to obtain $I_{o_{STC}}$. This requires careful analysis of these equations to determine the one that produces the best results in the replication of the experimental data. However, these equations depend on I_{ph}, R_s, R_{sh} and n, which are unknown parameters that must be determined first.

4.3. Ideality Factor (n)

The ideality factor can be evaluated as a function of series ad shunt resistances or by considering their extreme values. Considering the approach we introduced in our previous work [48], in which the ideality factor was evaluated in the optimum ideality-factor neighborhood, in this paper we discuss further extraction of n for $0 \le n \le n_o$.

4.3.1. Ideality Factor (n) Dependence on R_s and R_{sh}

The exponential term $\exp(I_{sc}R_s/nN_sV_t)$, in the denominators of Equations ((13) and (15)) can be omitted, as it has insignificant value compared to the other exponential terms in the respective denominators. Therefore, Equations ((13) and (15)) can be written as

$$I_o = \frac{I_{sc}R_{sh} + I_{sc}R_s - V_{oc}}{R_{sh}\exp\left(\dfrac{V_{oc}}{nN_sV_t}\right)}. \tag{21}$$

and

$$I_o = \frac{I_{sc}R_s + I_{sc}R_{sh} - V_{mpp} - I_{mpp}R_{sh} - I_{mpp}R_s}{R_{sh}\exp\left(\dfrac{V_{mpp} + I_{mpp}R_s}{nN_sV_t}\right)}. \tag{22}$$

Equating Equations ((21) and (22)) and solving for n gives

$$n = \frac{V_{oc} - V_{mpp} - I_{mpp}R_s}{N_sV_t\left[\ln\left(\dfrac{I_{sc}R_{sh} + I_{sc}R_s - V_{oc}}{I_{sc}R_{sh} + I_{sc}R_s - I_{mpp}R_{sh} - I_{mpp}R_s - V_{mpp}}\right)\right]}. \tag{23}$$

4.3.2. Ideality Factor (n) Dependence on Extremum Values of R_s and R_{sh}

The ideality factor can also be derived simply by first removing the exponential terms using logarithm and subtracting Equations (4) and (5) to obtain

$$n = \frac{V_{oc} - V_{mpp} - I_{mpp}R_s}{N_s V_t \left[\ln\left(\dfrac{I_{ph} + I_o - \dfrac{V_{oc}}{R_{sh}}}{I_{ph} + I_o - I_{mpp} - \dfrac{V_{mpp} + I_{mpp}R_s}{R_{sh}}} \right) \right]}. \quad (24)$$

In Equation (24) the ideality factor relates with I_{ph}, I_o, R_s and R_{sh} at both maximum power point (I_{mpp}, V_{mpp}) and open circuit point (V_{oc}). For initial estimates, the R_s *and* R_{sh} values can be ignored in both the numerator and denominator. They have very small and very large values, where $R_s \approx 0$ and $R_{sh} \approx \infty$, respectively. This makes it possible to introduce the short circuit point into Equation (24) since the photocurrent relationship given in Equation (3) reduces to $I_{ph} \approx I_{sc}$. Therefore, the ideality factor can be evaluated with respect to saturation current and the three crucial points as

$$n = \frac{V_{oc} - V_{mpp}}{N_s V_t \left[\ln\left(\dfrac{I_{sc} + I_o}{I_{sc} + I_o - I_{mpp}} \right) \right]}. \quad (25)$$

This assumption gives n_o in terms of I_{sc}, I_{mpp}, V_{oc} and V_{mpp} only. Hence,

$$n_o = \frac{V_{oc} - V_{mpp}}{N_s V_t \left[\ln\left(\dfrac{I_{sc}}{I_{sc} - I_{mpp}} \right) \right]}. \quad (26)$$

4.4. Shunt Resistance (R_{sh}) and Series Resistance (R_s)

The values of shunt and series resistance can be evaluated using the equations derived using I_{sc}, I_{mpp}, V_{mpp} and V_{oc} through an iterative process. Using I_{mpp} and V_{mpp} the relationship between R_{sh} *and* R_s *can* be evaluated by rearranging Equation (5) to obtain

$$R_{sh} = \frac{V_{mpp} + I_{mpp}R_s}{I_{ph} - I_{mpp} - I_o\left(\exp\left(\dfrac{V_{mpp} + I_{mpp}R_s}{nN_s V_t} \right) - 1 \right)}. \quad (27)$$

The combination of Equations (3) and (4) gives a relation between R_{sh} and R_s in terms of I_{sc} and V_{oc} given by

$$R_{sh} = \frac{V_{oc} - I_{sc}R_s}{I_{sc} + I_o \exp\left(\dfrac{I_{sc}R_s}{nN_s V_t} \right) - I_o \exp\left(\dfrac{V_{oc}}{nN_s V_t} \right)}. \quad (28)$$

Similarly, the combination of Equations ((3) and (5)) gives a relation between R_{sh} and R_s *in* terms of I_{sc}, I_{mpp} and V_{mpp} to obtain

$$R_{sh} = \frac{V_{mpp} + I_{mpp}R_s - I_{sc}R_s}{I_{sc} - I_{mpp} - I_o \exp\left(\dfrac{V_{mpp} + I_{mpp}R_s}{nN_s V_t} \right) + I_o \exp\left(\dfrac{I_{sc}R_s}{nN_s V_t} \right)}. \quad (29)$$

Again, merging Equations ((4) and (5)) yields

$$R_{sh} = \frac{V_{oc} - V_{mpp} - I_{mpp}R_s}{I_{mpp} + I_o \exp\left(\frac{V_{mpp} + I_{mpp}R_s}{nN_sV_t}\right) - I_o \exp\left(\frac{V_{oc}}{nN_sV_t}\right)}. \quad (30)$$

Shunt resistance (R_{sh}) and series resistance (R_s) can also be analyzed using the vanishing slope of the output power at maximum power point of Equation (1) and derivatives at short circuit and open circuit points with respect to V [12] [27] [49] [50] [51].

The derivative of Equation (1) with respect to V gives

$$\frac{\partial I}{\partial V} = -\frac{I_o}{nN_sV_t}\left\{\left(1 + \frac{\partial I}{\partial V}R_s\right)\exp\left(\frac{V + IR_s}{nN_sV_t}\right)\right\} - \frac{1}{R_{sh}}\left(1 + \frac{\partial I}{\partial V}R_s\right). \quad (31)$$

The derivative at short circuit point gives

$$\left[\frac{\partial I}{\partial V}\right]_{I=I_{sc}} = -\frac{1}{R_{sh}}. \quad (32)$$

and at open circuit point

$$\left[\frac{\partial I}{\partial V}\right]_{V=V_{oc}} = -\frac{1}{R_s}. \quad (33)$$

At maximum power point the power derivative with respect to voltage can be evaluated as

$$\left[\frac{\partial P}{\partial V}\right] = \left(\frac{\partial I}{\partial V}\right)V + I = 0. \quad (34)$$

At maximum power point the power derivative with respect to voltage can be evaluated as

$$-\frac{I_{mpp}}{V_{mpp}} = -\frac{I_o}{nN_sV_t}\left\{\left(1 - \frac{I_{mpp}}{V_{mpp}}R_s\right)\exp\left(\frac{V_{mpp} + I_{mpp}R_s}{nN_sV_t}\right)\right\} - \frac{1}{R_{sh}}\left(1 + \frac{I_{mpp}}{V_{mpp}}R_s\right). \quad (35)$$

By rearranging Equation (35) we can obtain

$$R_{sh} = \frac{V_{mpp} - I_{mpp}R_s}{I_{mpp} - \frac{I_o}{nN_sV_t}\left(V_{mpp} + I_{mpp}R_s\right)\exp\left(\frac{V_{mpp} + I_{mpp}R_s}{nN_sV_t}\right)}. \quad (36)$$

4.4.1. Evaluation and Analysis of R_{sh} and R_s Pairs

This paper presents a simplified analytical approach for evaluating and analyzing R_{sh} and R_s pairs. Considering Equations ((27)-(30) and (36)), there are only three unknown parameters, *i.e.*, R_s, the ideality factor and saturation current that appears on the right hand side of each equation. The saturation current has been derived in Equations ((14), (16) and (18)) with respect to ideality factor. A simple mathematical analysis can be done by replacing I_o in Equations ((27)-(30) and (36)) using Equation (14) to remain with ideality factor as the only unknown parameter. Comparing Equations ((27)-(30) and (36)), only Equation (30) that gives positive values of R_{sh} and R_s pairs after replacing I_o with Equation (14). Therefore, eliminating I_o of Equation (30) using (14) gives

$$R_{sh} = \frac{V_{oc} - V_{mpp} - I_{mpp}R_s}{I_{mpp} - I_{sc} + I_{sc}\exp\left(\frac{V_{mpp} + I_{mpp}R_s - V_{oc}}{nN_sV_t}\right)}. \quad (37)$$

Equation (37) can be analyzed using an iterative approach to obtain the [R_s, R_{sh}] pairs by selecting the values of n that are less than n_o. As introduced by [52], the R_s and R_{sh} limits can be calculated using

$$R_{sh_{\max}} = \frac{V_{oc} - V_{mpp}}{I_{mpp}}. \quad (38)$$

and

$$R_{sh_{\min}} = \frac{V_{mpp}}{I_{sc} - I_{mpp}} - R_{s_{\max}}. \quad (39)$$

Limiting the ideality factor selection within the $0 \le n \le n_o$ range and setting R_s and R_{sh} limits given by Equations ((38) and (39)) respectively, makes the process fast and robust. In addition, the ideality factor is selected in order to get an R_s and R_{sh} pair that guarantees the simulated maximum power ($P_{mpp}(sim)$) matches maximum power obtained experimentally, where $P_{mpp}(expt) = I_{mpp} * V_{mpp}$. The $P_{mpp}(sim)$ relationship can be derived by replacing $I = I_{mpp}$ and $V = V_{mpp}$ in Equation (1) to yield

$$P_{mpp}(sim) = V_{mpp}\left(I_{ph} - I_o\left(\exp\frac{V_{mpp} + I_{mpp}R_s}{nN_sV_t} - 1\right) - \frac{V_{mpp} + I_{mpp}R_s}{R_{sh}}\right) = P_{mpp}(expt). \quad (40)$$

The value of I_{ph} in Equation (40) can be replaced using Equation (3) by letting the term $I_o \exp\left(I_{sc}R_s / nN_sV_t\right) \approx 0$, since it has insignificant value compared to the other terms. Thus we can rewrite,

$$I_{ph} = I_{sc} + \frac{I_{sc}R_s}{R_{sh}}. \quad (41)$$

Further, the saturation current in Equation (40) can be replaced by Equation (16) to obtain

$$\begin{aligned} &P_{mpp}(sim) \\ &= V_{mpp}\left(\left(I_{sc} + \frac{I_{sc}R_s}{R_{sh}}\right) - \left(\frac{I_{sc} - I_{mpp}}{\exp\left(\frac{V_{mpp}}{nN_sV_t}\right)}\right)\left(\exp\frac{V_{mpp} + I_{mpp}R_s}{nN_sV_t} - 1\right) - \frac{V_{mpp} + I_{mpp}R_s}{R_{sh}}\right) \\ &= P_{mpp}(expt) \end{aligned} \quad (42)$$

Both Equations (37) and (42) can be solved simultaneous by arbitrarily selecting ideality factor below n_o and by increasing the values of R_s from zero to $R_{s_{\max}}$ using computer software. This process is repeated until the value of simulated maximum power ($P_{mpp}(sim)$) matches maximum power obtained experimentally $P_{mpp}(expt)$ or has an error margin of less than 0.5% [53].

The percentage error in power can be expressed as

$$P_{mpp}Error = \Delta P_{mpp}\% = \frac{P_{mpp} - I_{mpp}R_s}{I_{mpp}V_{mpp}}. \quad (43)$$

4.4.2. Extraction of Ideality Factor n, R_s and R_{sh} Using an Iterative Computational Process

The values of n, R_s and R_{sh} can be extracted using an iterative process using Equation (37) and verified using both Equations ((42) and (43)). The ideality factor is arbitrarily chosen starting from $n \le n_0$ [52] in steps of −0.001 and applied in Equation (37) to obtain [R_s, R_{sh}] pair. Subsequently, in the iterative stage, these n, R_s, and R_{sh} values are used in Equation (42) until the trio that satisfies $P_{mpp}(sim) \equiv P_{mpp}(expt)$ is achieved.

4.4.3. Simulation of R_{sh} and R_s Pairs

Table 1 provides a summary of data from the KC200GT datasheet profile and experimental data for Solinc 120 W measured using Gsola XJCM-10A solar simulator that has been used to simulate R_{sh} and R_s pairs. Figure 2 illustrates the R_{sh} and R_s relationship given by Equation (37) and has been sketched using data presented in Table 1.

The optimum ideality factors and optimum saturation current are also listed in Table 1. The optimum ideality factors values have been determined using Equation (26). Similarly, the optimal saturation current has been determined using Equation (14). These optimal values set the limit for both ideality factor and saturation current but they do not give the best results when plotting the I-V and P-V curves. This leads to further analysis of ideality factors near the optimal values and their respective saturation current.

Table 2 gives a summary of ideality factor n, R_s, R_{sh}, I_o and I_{ph} parameters for Solinc 120 W and Kyocera KC200GT solar modules. The main aim has been to use the available information for I_{sc}, I_{mpp}, V_{oc} *and* V_{mpp} *to* arrive at most appropriate values listed in Table 2**.** These values have been used as the starting figures for I-V relationship as demonstrated in the following section.

5. Improved Analysis of Current-Voltage Relationship for Five-Parameter Model Using Newton-Raphson Technique

The previous sections have demonstrated a simplified approach of obtaining the

Table 1. Solinc 120 W and Kyocera KC200GT photovoltaic modules data at STC.

Parameters	Solinc 120 W	KC200GT
I_{mpp} (A)	7.1814	7.61
V_{mpp} (V)	16.905	26.3
I_{sc} (A)	7.59995	8.21
V_{oc} (V)	21.529	32.9
N_s	36	54
n_o	1.72529	1.81928
$I_{o\text{-}opt}$ (A)	1.0439E−05	1.7807E−5

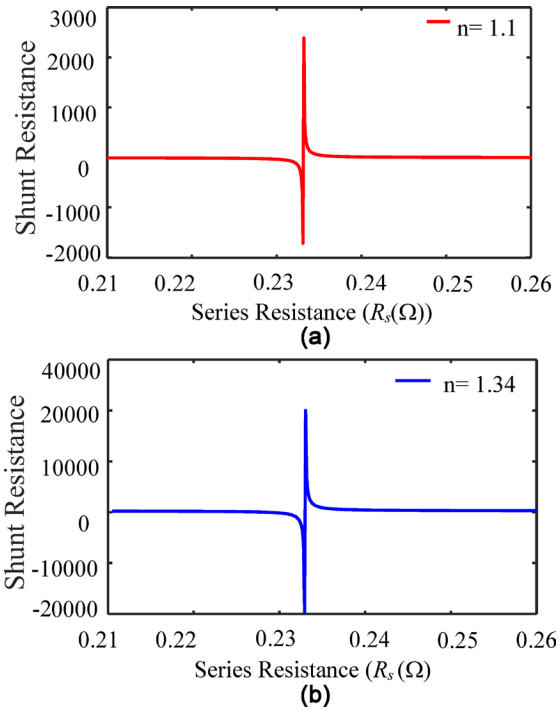

Figure 2. A graph of R_{sh} versus R_s at STC for (a) Solinc 120 W from solar simulator values and (b) for KC200GT from datasheet values.

Table 2. Extracted parameters for Solinc 120 W and Kyocera KC200GT photovoltaic modules using equations (37) and (42).

Parameters	Solinc 120 W	KC200GT
n	1.1	1.34
R_s (Ω)	0.236	0.214
R_{sh} (Ω)	3746.809	525.145
I_o (A)	4.9089E−09	1.6936E−07
I_{ph} (A)	7.59995	8.2297

model parameters. The approach heavily depended on the values of I_{sc}, I_{mpp}, V_{oc} and V_{mpp}; the main cardinal points. This can be considered as a rough understanding of the solution of Equation (1). We have thus applied Newton-Raphson technique to iteratively solve Equation (1) in order to consider all points in characterization of photovoltaic modules using I-V and P-V curves. The Newton-Raphson technique is based on estimation of a given function $f(I) = 0$ [54].

We can rearrange Equation (1) as,

$$f(I) = I_{ph} - I_o\left[\exp\left(\frac{V+IR_s}{nN_sV_t}\right)-1\right]-\frac{V+IR_s}{R_{sh}}-I=0\,. \tag{44}$$

Differentiating Equation (44) with. respect to Ileads to

$$\frac{\partial\left(f(I)\right)}{\partial I} = -\frac{I_oR_s}{nN_sV_t}\left[\exp\left(\frac{V+IR_s}{nN_sV_t}\right)\right]-\frac{R_s}{R_{sh}}-1\,. \tag{45}$$

Therefore, we can apply Equations (44) and (45) to implement the Newton-Raphson approach and obtain

$$I_{j+1} = I_j - \frac{f\left(I_j\right)}{\frac{\partial\left(f\left(I_j\right)\right)}{\partial I}} = I_j - \frac{I_{ph} - I_o\left[\exp\left(\frac{V + I_j R_s}{nN_s V_t}\right) - 1\right] - \frac{V + I_j R_s}{R_{sh}} - I_j}{-\frac{I_o R_s}{nN_s V_t}\left[\exp\left(\frac{V + I_j R_s}{nN_s V_t}\right)\right] - \frac{R_s}{R_{sh}} - 1} \quad (46)$$

where, j represents the number of iterative process.

Equations (44)-(46) require initial values of n and R_s. In this paper, we introduce the new approach presented in section 4.4 that easily determines the trio values of n, R_s and R_{sh}. These values are also used to calculate I_o and I_{ph}. Implementation of all five parameter values in Equations (44)-(46) reduces the number of iterative processes needed to obtain the most suitable I and V values, thereby increasing the computation speed.

The identified values of I and V are applied in the power equation given by

$$P = I_{ph}V - I_o V\left[\exp\left(\frac{V + IR_s}{nN_s V_t}\right) - 1\right] - \frac{V^2}{R_{sh}} - VI\frac{R_s}{R_{sh}}. \quad (47)$$

5.1. Analysis of Different Approaches for Extracting Five-Model Parameters

All the five parameters in Table 2 for Solinc 120 W and KC200GT modules that have been deduced using the new simplified simulation procedure are applied in solving Equation (46) to obtain a good approximation of the output current. This approach offers a simple and very efficient calculation procedure for all current and voltage values starting from $I = 0$ to $I = I_{sc}$ and $V = 0$ to $V = V_{oc}$. It offers very precise solutions for all the points needed to plot the I-V and P-V or P-I curves.

In this work, we have classified four most suitable data extraction approaches for determining I and V using Newton-Raphson method. These categories depend on the choice of saturation current equations discussed in section 4.2 and 4.3.1. Category 1 is based on saturation currents that are dependent on R_s and R_{sh} resistances at open and short circuit points (SCDR-OS) where I_o is calculated using Equations ((11), (13) and (21)). Category 2 is based on saturation current that is independent of R_s and R_{sh} resistances at open and short circuit points (SCIR-OS), where I_o is calculated using Equations ((12) and (14)). Categories 3 and 4 are based on saturation currents at both open circuit and maximum power points that are dependent on R_s and R_{sh} resistances (SCDR-OMP) and saturation currents that are independent of R_s and R_{sh} resistances (SCIR-OMP), where the I_os are calculated using Equations ((17) and (18)) respectively. The use of saturation current defined by Equations ((9), (10), (15), (16) and (22)) does, however, provide unsatisfactory data for I and V.

These procedures can be implemented using the algorithm shown in Figure 4 which outlines all the steps required to retrieve the data for plotting the I-V and

P-V curves as follows.

- The process starts with input values of I_{sc}, I_{mpp}, V_{mpp}, V_{oc}, N_s and V_t from Table 1.
- Followed by setting the number of iterations, NiMax for current approximation and NvMax for voltage resolution plus precision description for R_s increment defined by *Rsinc*.
- The algorithm presented in Figure 3 is then applied to obtain n, R_s and R_{sh} values.
- These n, R_s and R_{sh} are used to calculate I_o and I_{ph} for the first iteration of determining the current and voltage data.
- The process is repeated severally for each iteration with an increment of R_s ($R_s = R_s + Rsinc$) until NiMax and NvMax are reached by solving Equations (44)-(46).
- The P-error is then evaluated to determine the most suitable values for n, R_s, R_{sh}, I_o and I_{ph} which give the best current, voltage and power data.
- If the error in power is greater than 0.5%, the process is repeated by inputting a new value of ideality actor.
- Finally, the process ends by plotting I-V and P-V curves and the cardinal point markers if the error in power is less or equal to 0.5%.

5.2. Evaluation of Extracted Parameters for Solinc 120 W and KC200GT Modules Using the Four Approaches

Table 3 & Table 4 display the five-model parameter data for Solinc 120 W and

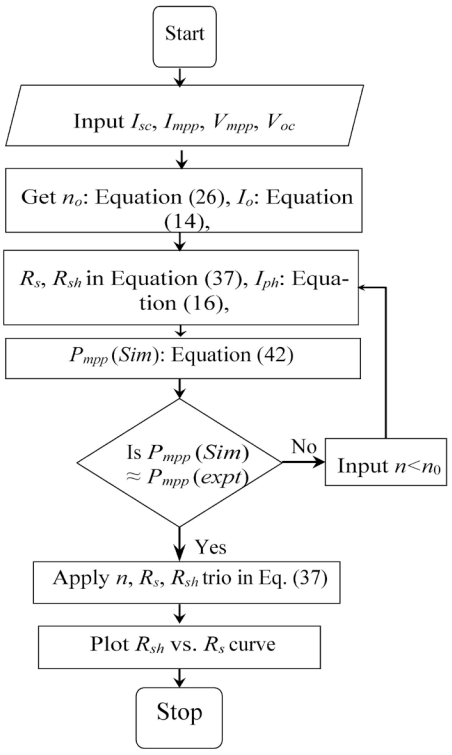

Figure 3. An algorithm for evaluating the n, R_s and R_{sh} using I_{sc}, I_{mpp}, V_{mpp} and V_{oc}.

Table 3. Simulated data for Solinc 120, where I_o has been calculated using approach 1 of Equations ((11), (13) or (21)), approach 2 of Equations ((12) or (14)), approach 3 Equation (17) and approach 4 Equation (18).

Parameters	Equations for $\{R_s, R_{sh}\}$pair	Series Resistance (R_s (Ω))	Shunt Resistance (R_{sh} (Ω))	Ideality Factor (n)	Saturation Current ($I_o \times 10^{-9}$ (A))	Photo Current (I_{ph} (A))	Power (P_{mpp} (W))	Change in Power (ΔP_{mpp} %)
Approach 1	(27)	0.233	6694.87	1.1	4.8984	7.6014	121.463	0.0456
	(29)	0.233	6943.00	1.1	4.8857	7.6032	121.505	0.0844
Approach 2	(27)	0.233	3746.81	1.1	4.9089	7.6045	121.457	0.0444
	(28)	0.233	706,150,048	1.1	4.9089	7.6000	121.464	0.0503
	(29)	0.233	37,898.74	1.1	4.9089	7.6003	121.462	0.0486
	(30)	0.233	−6653.75	1.1	4.9089	7.6443	122.190	0.6481
	(36)	0.255	−279.34	1.1	4.9089	7.6485	122.056	0.5380
Approach 3	(27)	0.233	3054.06	1.1	4.9009	7.6049	121.458	0.0452
	(28)	0.233	240.07	1.1	4.8557	7.6443	121.026	−0.3105
	(29)	0.233	23,248.547	1.1	4.9056	7.6008	121.469	0.0548
	(36)	0.254	12,008.21	1.1	4.9036	7.6483	121.082	−0.2642
Approach 4	(27)	0.2395	18,565.30	1.1	4.6883	7.6005	121.459	0.0280
	(28)	0.1501	59.71	1.1	4.6883	7.6286	121.319	−0.0416
	(29)	0.2395	34,945.22	1.1	4.6883	7.6000	121.459	0.0283
	(36)	0.2608	6726.41	1.1	4.6883	7.6496	121.062	−0.1704

Table 4. Simulated data for KC200GT, where Io has been calculated using approach 1 of equations (11), (13) or (21), approach 2 of equations (12) or (14), approach 3 Equation (17) and approach 4 Equation (18).

Parameters	Equations for $\{R_s, R_{sh}\}$ pair	Series Resistance (R_s (Ω))	Shunt Resistance (R_{sh} (Ω))	Ideality Factor (n)	Saturation Current ($I_o \times 10^{-7}$ (A))	Photo Current (I_{ph} (A))	Power (P_{mpp} (W))	Change in Power (ΔP_{mpp} %)
Approach 1	(27)	0.2187	712.83	1.34	1.6671	8.2174	200.143	0.000018
	(29)	0.2187	904.25	1.34	1.6755	8.2151	200.218	0.0377
Approach 2	(27)	0.2134	367.85	1.34	1.6936	8.2508	200.143	0.000015
	(28)	0.2134	71,669,727	1.34	1.6936	8.2100	201.013	0.4345
	(29)	0.2134	744.51	1.34	1.6936	8.2124	200.144	0.00051
	(30)	0.2283	13,153.36	1.34	1.6936	8.2100	200.076	−0.0335
	(36)	0.2165	1013.88	1.34	1.6936	8.2120	200.200	0.0283
Approach 3	(27)	0.2161	749.58	1.34	1.6840	8.2152	200.143	0.000016
	(28)	0.2161	200.48	1.34	1.6616	8.2513	198.701	−0.72038
	(29)	0.2282	1,367,493	1.34	1.6932	8.2107	200.152	0.0045
	(36)	0.2198	379.03	1.34	1.6637	8.252	200.108	−0.0176
Approach 4	(27)	0.2258	368.61	1.34	1.6163	8.2531	200.143	0.000007
	(28)	0.1002	85.55	1.34	1.6163	8.2196	199.970	−0.0862
	(29)	0.2279	934.82	1.34	1.6163	8.2120	200.143	0.000014
	(36)	0.2289	1068.57	1.34	1.6163	8.212	200.176	0.0165

KC200GT solar modules and their simulated output power and errors. The following sections discuss the most realistic results of the five-model parameter that provide more practical data for each approach that fits experimental results. Four approaches are listed here since they give small percentage error.

***Approach* 1**

The data shown in Table 3 & Table 4 in rows 2 - 3 summarizes the Solinc 120W and KC200GT parameters that have been extracted from the first category of data procedure. These data are based on open and short circuit points, where I_o is determined using Equations ((11), (13) or (21)). However, this category only gives a satisfying [R_s, R_{sh}] pair from Equations ((27) and (29)).

***Approach* 2**

The data shown in Table 3 & Table 4 in rows 4 - 8, give category 2 data for Solinc 120 W and KC200GT where I_o has been calculated using either Equations (12) or (14) that are independent of R_s, R_{sh} pair. This category gives satisfactory

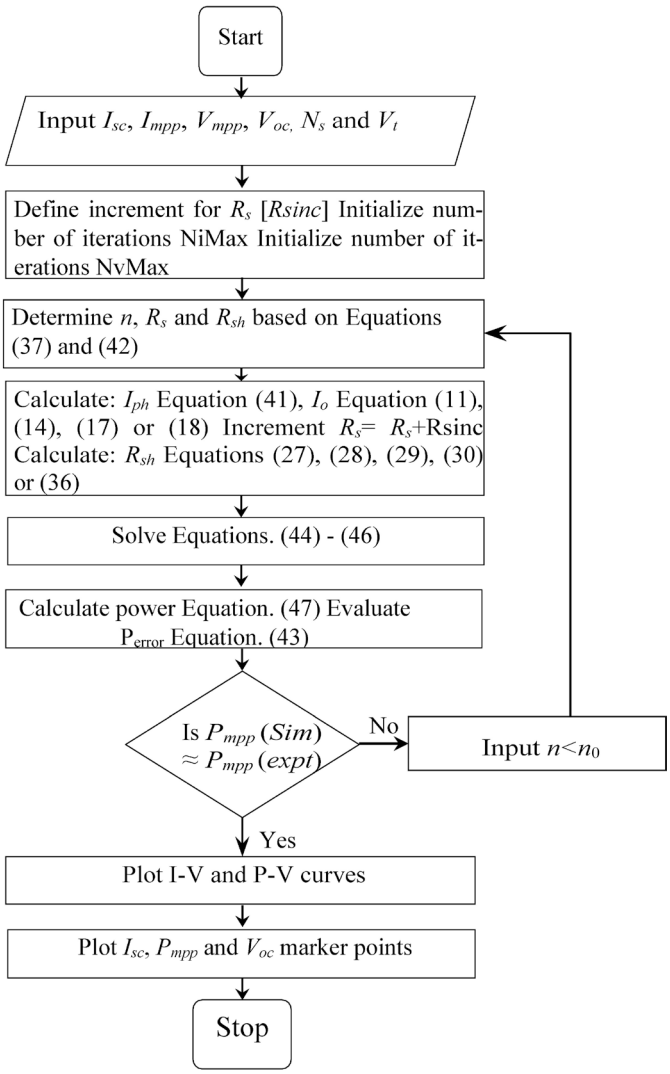

Figure 4. An algorithm for calculating current (I) using Newton-Raphson technique and plotting I-V and P-V curves.

[R_s, R_{sh}] pair from Equations ((27), (28) (29), (30) and (36)).

***Approach* 3**

Again, the data shown in Table 3 & Table 4 in rows 9 - 12, represent category 3 where I_o is determined using Equation (17). This category gives satisfactory [R_s, R_{sh}] pair only from Equations ((27), (28), (29) and (36)).

***Approach* 4**

Finally, rows 13 - 16 of Table 3 & Table 4 give category 4 data for Solinc 120 W and KC200GT, where I_o is determined using Equation (18) that is independent of R_s, R_{sh} pair. This category also gives satisfactory [R_s, R_{sh}] pair only from Equations ((27), (28), (29) and (36)).

It is clear from Table 3 & Table 4 that the saturation current (I_o) calculated using Equations ((12) or (14)) in approach 2 gives acceptable ΔP_{mpp} errors when applied to all R_{sh} Equations ((27)-(30), or (36)).

Approach 1 gives satisfactory data when applied in Equations ((27) and (29)). Other approaches, 3 and 4 give reasonable results when applied in Equations ((27), (28), (29) and (36)). Evidently, Equations ((27) and (29)) that have been derived at maximum power point and combination of maximum power point and short circuit equations, respectively, give the best results of ΔP_{mpp} error for all saturation current equations at constant ideality factor. Equation (28) gives very large and very small values of R_{sh} when applied in approaches 2 and 4. All the four approaches give satisfactory data when compared with other methods reported by different authors as demonstrated in Table 5 & Table 6.

These data are summarized in Table 5 for R_{sh} of Equation (27) that gives the smallest error for each approach. Approach 1 data and data from [52] have similar results while approaches 2 and 3 have different R_{sh} values for the same R_s = 0.233 Ω. However, approach 4 has R_s = 0.2395 Ω that gives the least ΔP_{mpp} error and very large value of R_{sh} = 18,565 Ω. Analytical approach reported by [41] provides satisfactory parameters that are closer to the values obtained using the four approaches.

The values of five-model parameters obtained using approaches discussed in the works of [41] [52] have been compared with the values of parameters for

Table 5. Comparison of calculated parameters with other approaches in literature for Solinc 120 W.

Parameters	Series Resistance (R_s (Ω))	Shunt Resistance (R_{sh} (Ω))	Ideality Factor (n)	Saturation Current ($I_o \times 10^{-9}$ (A))	Photo Current (I_{ph} (A))
Approach 1	0.233	6694.87	1.1	4.5915	7.6014
Approach 2	0.233	3746.81	1.1	4.9089	7.6045
Approach 3	0.233	3054.06	1.1	4.9009	7.6049
Approach 4	0.2395	18,565.30	1.1	4.6883	7.6005
[52] approach	0.233	6694.87	1.1	4.8984	7.6014
[41] approach	0.264	16,400.11	1.1	4.5915	7.6502

Table 6. Comparison of calculated parameters with other approaches in literature for KC200GT.

Parameters	Series Resistance (R_s (Ω))	Shunt Resistance (R_{sh} (Ω))	Ideality Factor (n)	Saturation Current (I_o (A))	Photo Current (I_{ph} (A))
Approach 1	0.2187	712.83	1.34	1.667E−07	8.2174
Approach 2	0.2134	367.85	1.34	1.694E−07	8.2508
Approach 3	0.2161	749.58	1.34	1.684E−07	8.2152
Approach 4	0.2258	368.61	1.34	1.616E−07	8.2531
Data by [40]	0.217	951.927	1.34	1.7100E−7	8.212
Data by [52]	0.221	415.405	1.3	9.825E−8	8.214
Data by [50]	0.231	594.851	1.3	9.6990E−8	8.213
Data by [41]	0.217	951.92	1.342	1.71E−7	8.211
Data by [51]	0.2108	145.083	1.1578	1.01E−8	8.226
Data by [38]	0.21095	192.757	1.1482	8.6369E−9	8.218985

Solinc 120 W using approaches 1 - 4 of Table 3.

These data are summarized in Table 5 for R_{sh} of Equation (27) that gives the smallest error for each approach. Approach 1 data and data from [52] have similar results while approaches 2 and 3 have different R_{sh} values for the same R_s = 0.233 Ω. However, approach 4 has R_s = 0.2395 Ω that gives the least ΔP_{mpp} error and very large value of R_{sh} = 18565 Ω. Analytical approach reported by [41] provides satisfactory parameters that are closer to the values obtained using the four approaches.

The results obtained using analytical methods published by [38] [40] [41] [50] [51] [52] have been compared with the KC200GT parameters values in Table 4 and summarized in Table 6. The values of R_s obtained using the four methods discussed in this work are consistent with their analysis within ±0.02 Ω. All parameter values shown in Table 4 provide satisfactory results for output power within the error margin given by the manufacturer of +10% or −5%. A typical way of testing the 5-parameter model is through I-V and P-V plots.

6. I-V and P-V Characterization for Solinc 120 W and KC200GT Photovoltaic Modules Based on the Four Approaches at STC

The values of simulated parameters listed in Table 5 & Table 6 for Solinc 120 W and KC200GT, have been used to plot the I-V and P-V curves at standard test condition.

Figure 5 shows the current-voltage relationship for Solinc 120 W, in which the zoomed parts illustrate the short circuit, maximum power and open circuit points for all the four approaches. The curves converge at maximum power point but vary significantly at the point of short circuit and at the point of open circuit. The second approach gives the best replica of these cardinal points.

Figure 6 shows the power-voltage relationship for Solinc 120 W solar module, in which the zoomed sections show the areas surrounding the maximum power and the open circuit points. The zoomed sections show the differences between the four approaches, which is a reflection of the values of errors given in Table 4.

The current-voltage relationship for KC200GT is shown in Figure 7, in which the zoomed sections represent the short circuit, maximum power and open circuit points. The curves converge at maximum power point but vary greatly at the point of the short circuit and at the point of the open circuit. Again, the second method offers the best possible representation of these cardinal points.

Figure 8 displays the power-voltage relationship for KC200GT solar module, in which the zoomed parts represent the areas surrounding the maximum power and the open circuit points. The zoomed sections display the differences between the four methods, which is a representation of error values given in Table 5. According to the I-V and P-V plots of Figures 5-8, the four analytical approaches give satisfactory parameters values for a single diode model that matches the experimental data and manufacturer's profile.

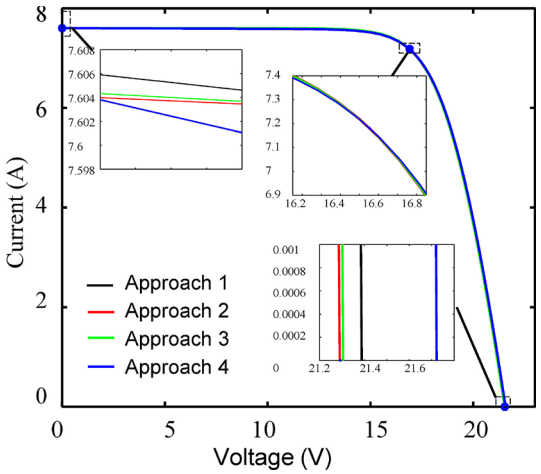

Figure 5. A graph of current versus voltage for Solinc 120 W at STC.

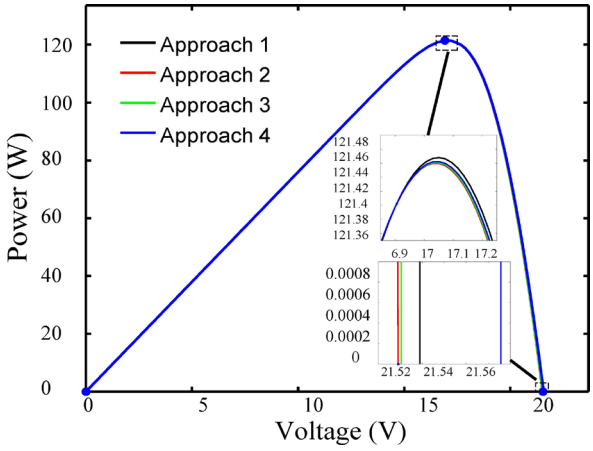

Figure 6. A graph of power versus s voltage for Solinc 120 W at STC.

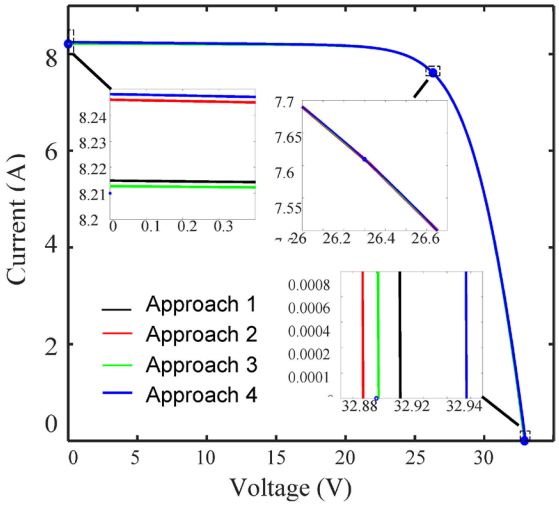

Figure 7. A graph of current versus s voltage for KC200GT at STC.

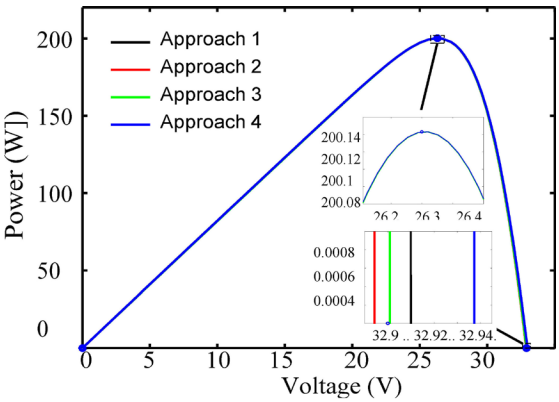

Figure 8. A graph of power versus voltage for KC200GT at STC.

7. I-V and P-V Characterization at Ambient Temperature, NOCT and Actual Irradiance

The effects of the actual solar irradiation (s_a) and module's surface temperature T on five-model parameters have been recently studied at open circuit, closed circuit and maximum power points [38] [51].

Starting with the cardinal points, the short circuit current can be determined using

$$I_{sc}\left(s_a,T\right)=\frac{s_a}{s_{STC}}\left[I_{sc\,STC}+K_{I_{sc}}\left(T-T_{STC}\right)\right] \tag{48}$$

where, $K_{I_{sc}}$ is the temperature coefficient of I_{sc} in A/˚C that is usually provided in manufacturer's data sheet. The maximum power-point current can be determined using

$$I_{mpp}\left(s_a,T\right)=\frac{s_a}{s_{STC}}\left[I_{mpp\,STC}+K_{I_{smpp}}\left(T-T_{STC}\right)\right] \tag{49}$$

where, $K_{I_{mpp}}$ is the temperature coefficient of I_{mpp} in A/˚C. Unlike $K_{I_{sc}}$, the manufacturer's data sheet does not include $K_{I_{mpp}}$. This can be evaluated by

simply applying the data at both STC and NOCT.

Manufacturers of solar modules with ISO/IEC International Standard provide, nominal operation cell temperature (NOCT) values at 800 W/m^2 at 20˚C [55] [56]. This can be used to relate the module temperature (T) with the actual irradiance and the air temperature (T_a) using

$$T = T_a + \frac{[T_{NOCT} - 20]s_a}{800} \tag{50}$$

For maximum power-point voltage a more robust analytical approach has been recently used by [38], in which

$$V_{mpp}(s_a, T) = V_{mpp_{STC}} + K_{v_{mpp}}(T - T_{STC}) + \alpha_{v_{mpp}}(s_a - s_{STC}) + \beta_{v_{mpp}}(s_a - s_{STC})^2 \tag{51}$$

where, $\alpha_{V_{mpp}}$ and $\beta_{V_{mpp}}$ are solar radiation coefficients at maximum-power point. Similarly, the short-circuit voltage can be evaluated as

$$V_{oc}(s_a, T) = V_{oc_{STC}} + K_{v_{oc}}(T - T_{STC}) + \alpha_{V_{oc}}(s_a - s_{STC}) + \beta_{V_{oc}}(s_a - s_{STC})^2 \tag{52}$$

where $\alpha_{V_{oc}}$, $\beta_{V_{oc}}$ are solar radiation coefficients at open circuit point.

Equations (51) and (52) are quadratic polynomials that require a careful extraction of the second-degree polynomial coefficients. In this paper, we have introduced a simpler approach for determining $V_{oc}(s_a, T)$ and $V_{mpp}(s_a, T)$ using

$$V_{oc}(s_a, T) = n(s_a, T) N_s V_t(T)\left[\ln\left(I_{sc}(s_a, T)\right) - \ln\left(I_o(s_a, T)\right)\right] \tag{53}$$

and,

$$V_{mpp}(s_a, T) = V_{oc}(s_a, T) - n_o N_s V_t(T) \times \left[\ln\left(\frac{I_{sc}(s_a, T)}{I_{sc}(s_a, T) - I_{mpp}(s_a, T)}\right)\right] \tag{54}$$

The saturation current dependence on module temperature can be achieved by rewriting Equation (20) as

$$I_o(s_a, T) = I_{o_{STC}}\left[\frac{T}{T_{STC}}\right]^3 \exp\frac{-qE_g}{n(s_a, T)N_s}\left(\frac{1}{T_{STC}} - \frac{1}{T}\right). \tag{55}$$

The temperature-dependent saturation current of Equation (55) can be compared with I_o of Equation (56), in which Equation (14) has been written as

$$I_o = \frac{I_{sc}(s_a, T)}{\exp\left(\frac{V_{oc}(s_a, T)}{n(s_a, T)N_s V_t(T)}\right)}. \tag{56}$$

Finally, the R_s and R_{sh} pair dependency on irradiance and temperature have been evaluated using Equation (27), by replacing its I_{ph}, I_o, I_{mpp} and V_{mpp} with values extracted using Equations ((7), (56), (49) and (54)) respectively.

The Kyocera KC200GT high-performance multi-crystal photovoltaic module with IEC standard has been used to demonstrate the effects of irradiance and temperature on main parameters of a single diode model as shown in **Table 7** & **Table 8**. The datasheet module offers nominal operating cell temperature data at 47˚C and 800 W/m^2 for the three cardinal points that have been used as starting

Table 7. Simulated data and extracted model parameters values for KC200GT photovoltaic module at air temperature of 20˚C and NOCT of 47˚C and different irradiance levels.

Irradiance (W/m^2)	200	400	600	800	1000
I_{sc} (A)	1.653	3.306	4.959	6.612	8.28
I_{mpp} (A)	1.533	3.066	4.599	6.132	7.665
V_{mpp} (V)	20.134	21.518	22.327	22.901	23.412
V_{mpp} (V) Ref. [38] method	21.549	22.295	22.822	23.130	23.220
V_{oc} (V)	27.239	28.623	29.432	30.006	30.455
V_{oc} (V) Ref. [38] method	28.062	28.818	29.425	29.884	30.194
n	1.1	1.12	1.28	1.32	1.34
$I_o \times 10^{-6}$ (A)	998.90	11.728	98.249	1.5618	1.9613
I_{ph} (A)	1.6564	3.3082	4.9629	6.6164	8.2844
R_s (Ω)	1.742	0.802	0.452	0.313	0.242
R_{sh} (Ω)	1750.956	555.481	2864.877	2235.484	6896.84
P_{mpp} (W)	30.924	66.098	102.814	140.574	179.561
ΔP_{mpp}%	0.1911	0.1879	0.1285	0.1037	0.0603

conditions to evaluate other parameters at various irradiances. In Table 7, the simulated $I_{sc}(s_a, T)$, $I_{mpp}(s_a, T)$, $V_{mpp}(s_a, T)$ and $V_{oc}(s_a, T)$ data have been applied in approach 2 discussed in section 5.1 to extracted $I_{ph}(s_a, T)$, $I_o(s_a, T)$, $n(s_a, T)$ $R_s(s_a, T)$ and $R_{sh}(s_a, T)$ and plot I-V and P-V curves at various irradiances.

The values of $\alpha_{V_{mpp}}$, $\alpha_{V_{oc}}$, $\beta_{V_{mpp}}$ and $\beta_{V_{oc}}$ presented in the supplementary data published by [38], have been applied to determine V_{mpp} and V_{oc} of equations (51) and (52). The simulated values of V_{oc} using Equation (53) and V_{mpp} using Equation (54) for irradiances chosen at 200, 400, 600, 800 and 1000 W/m^2, have been compared with the values obtained based on the [38] method as shown in Table 7. The data obtained using the new approaches are consistent with data simulated using [38] method. Figure 9 & Figure 10 illustrate the I-V and P-V curves at irradiances of 200, 400, 600, 800 and 1000 W/m^2, and air temperature of 20˚C and NOCT of 47˚C, while Figure 11 & Figure 12 show I-V and P-V curves at various temperatures.

8. Conclusions

In this report, we have considered photovoltaic systems operating at STC and various weather conditions and have presented two algorithms for extracting their five-model parameters based on a single-diode analogous circuit. The first algorithm plays an important role in deriving the unknown parameters to give a rough idea of their values that are used as preliminary data for the second algorithm based on Newton-Raphson numerical analysis method. This is a deviation from conventional methods, which assume initial arbitrary values.

In an attempt to establish the most comprehensive and simple procedure of arriving at the best five-model parameters, we categorized four approaches based

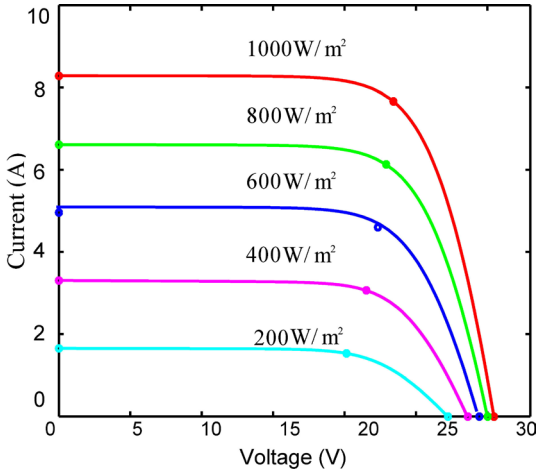

Figure 9. A graph of current versus voltage for KC200GT at air temperature of 20˚C and NOCT of 47˚C for various irradiances.

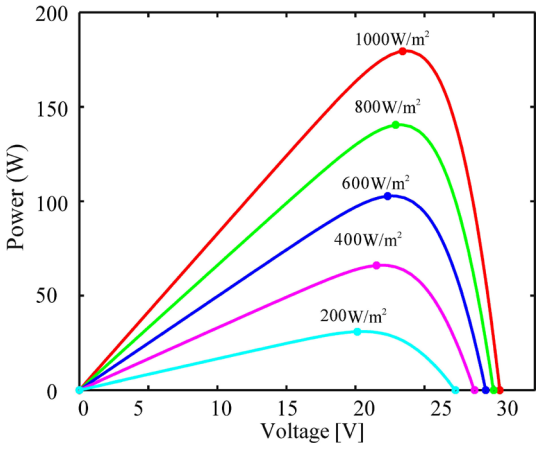

Figure 10. A graph of current versus voltage for KC200GT at air temperature of 20˚C and NOCT of 47˚C for various irradiances.

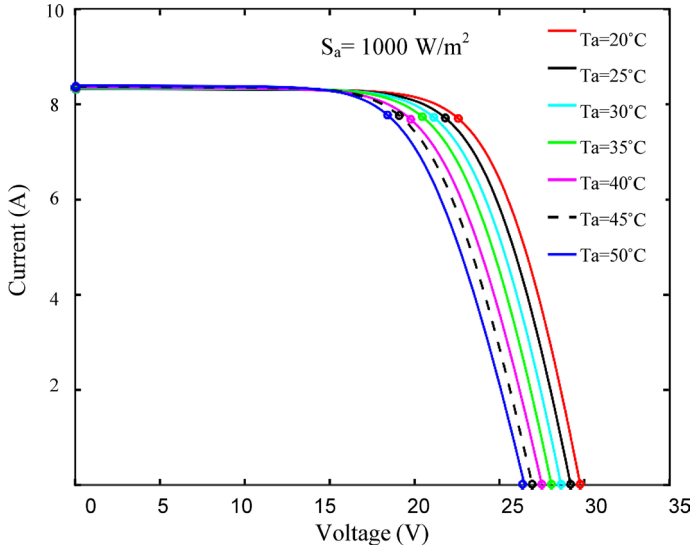

Figure 11. A graph of current versus voltage for KC200GT showing various temperatures curves at 1000 W/m².

Table 8. Simulated data and extracted model parameters values for KC200GT photovoltaic module at arbitrary air and NOCT temperatures for 1000 W/m^2.

T_a (˚C)	20	25	30	35	40	45	50
NOCT (˚C)	53.75	58.75	63.75	68.75	73.75	78.75	83.75
T (Kelvin)	326.9	331.9	336.9	341.9	346.9	351.9	356.9
I_{sc} (A)	8.3014	8.2944	8.3069	8.3194	8.3319	8.3444	8.3569
I_{mpp} (A)	7.6819	7.6944	7.7069	7.7194	7.6650	7.7444	7.7569
V_{mpp} (V)	22.522	21.758	21.079	20.399	19.717	19.034	18.350
V_{mpp} (V) *Ref.* [38] method	22.275	21.575	20.875	20.175	19.475	18.775	18.075
V_{oc} (V)	29.700	29.133	28.570	28.005	27.440	26.872	26.304
V_{oc} (V) *Ref.* [38] method	29.364	28.749	28.134	27.519	26.904	26.289	25.674
n	1.16	1.14	1.13	1.124	1.1	1.06	1.012
$I_o \times 10^{-6}$ (A)	40.682	54.031	82.299	1.3145	1.6203	1.577	1.2491
I_{ph} (A)	8.3120	8.3062	8.3199	8.334	8.3546	8.3642	8.3812
R_s(Ω)	0.332	0.352	0.363	0.371	0.412	0.418	0.468
R_{sh} (Ω)	913.865	928.483	925.197	831.949	437.605	726.471	814.787
P_{mpp} (W)	173.043	167.596	162.742	157.875	151.425	148.048	143.036
ΔP_{mpp}%	0.0191	0.1108	0.1787	0.2601	0.1940	0.4339	0.4901

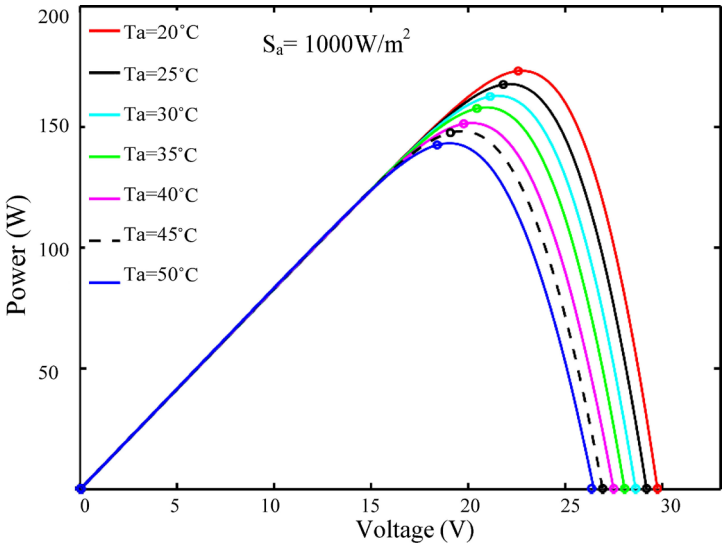

Figure 12. A graph of power versus voltage for KC200GT showing various temperatures curves at 1000 W/m^2.

of saturation-current relationships at the cardinal points of I-V plot. We considered the effect of shunt and series resistance on the saturation current at each key cardinal point or combination of two points, and found that dependence on the actual resistance induces a slight deviation of the saturation current as opposed to extreme resistance. When applied to the Newton-Raphson numerical analysis method, all four approaches provided satisfactory output current and

voltage values that match the experimental data or data presented in manufacturer's datasheet.

Beginning with the numerical values of the five-model parameters at STC, we simulated the five-model parameters at various irradiances and temperatures. We have presented new approaches to obtaining the V_{oc} and V_{mpp} at various irradiances and temperatures.

Acknowledgements

The authors would like to thank the Department of Physics and the Board of Graduate School; University of Nairobi (Kenya) for providing all the facilities and financial support respectively for this research.

Conflicts of Interest

The authors declare no conflicts of interest regarding the publication of this paper.

References

[1] Bórawski, P., Yashchenko, T., Sviderskyi, A. and Dunn, J.W. (2019) Development of Renewable Energy Market in the EU with Particular Regard to Solar Energy. *Conference Proceedings Determinants of Regional Development*, Pila, 12-13 April 2018, 43-55.

[2] Albini, A. and Rajnai, Z. (2019) Modeling General Energy Balance of Systems. *Procedia Manufacturing*, **32**, 374-379. https://doi.org/10.1016/j.promfg.2019.02.228

[3] Kabir, E., Kumar, P., Kumar, S., Adelodun, A.A. and Kim, K.H. (2018) Solar Energy: Potential and Future Prospects. *Renewable and Sustainable Energy Reviews*, **82**, 894-900. https://doi.org/10.1016/j.rser.2017.09.094

[4] Kannan, N. and Vakeesan, D. (2016) Solar Energy for Future World: A Review. *Renewable and Sustainable Energy Reviews*, **62**, 1092-1105. https://doi.org/10.1016/j.rser.2016.05.022

[5] Ishaque, K. and Salam, Z. (2013) A Review of Maximum Power Point Tracking Techniques of PV System for Uniform Insolation and Partial Shading Condition. *Renewable and Sustainable Energy Reviews*, **19**, 475-488. https://doi.org/10.1016/j.rser.2012.11.032

[6] Salas, V., Olias, E., Barrado, A. and Lazaro, A. (2006) Review of the Maximum Power Point Tracking Algorithms for Stand-Alone Photovoltaic Systems. *Solar Energy Materials and Solar Cells*, **90**, 1555-1578. https://doi.org/10.1016/j.solmat.2005.10.023

[7] Belhachat, F. and Larbes, C. (2018) A Review of Global Maximum Power Point Tracking Techniques of Photovoltaic System under Partial Shading Conditions. *Renewable and Sustainable Energy Reviews*, **92**, 513-553. https://doi.org/10.1016/j.rser.2018.04.094

[8] Nadia, A.R., Isa, N.A.M. and Desa, M.K.M. (2018) Advances in Solar Photovoltaic Tracking Systems: A Review. *Renewable and Sustainable Energy Reviews*, **82**, 2548-2569. https://doi.org/10.1016/j.rser.2017.09.077

[9] Hafez, A.Z., Yousef, A.M. and Harag, N.M. (2018) Solar Tracking Systems: Technologies and Trackers Drive Types: A Review. *Renewable and Sustainable Energy*

Reviews, **91**, 754-782. https://doi.org/10.1016/j.rser.2018.03.094

[10] Jiang, L.L., Srivatsan, R. and Maskell, D.L. (2018) Computational Intelligence Techniques for Maximum Power Point Tracking in PV Systems: A Review. *Renewable and Sustainable Energy Reviews*, **85**, 14-45. https://doi.org/10.1016/j.rser.2018.01.006

[11] Boukebbous, S.E. and Kerdoun, D. (2015) Study, Modeling and Simulation of Photovoltaic Panels under Uniform and Non-Uniform Illumination Conditions. *Revue des Energies Renouvelables*, **18**, 257-268.

[12] Kennerud, K.L. (1969) Analysis of Performance Degradation in CdS Solar Cells. *IEEE Transactions on Aerospace and Electronic Systems*, **6**, 912-917. https://doi.org/10.1109/TAES.1969.309966

[13] Otterbein, R.T., Evans, D.L. and Facinelli, W.A. (1978) A Modified Single Diode Model for High Illumination Solar Cells for Simulation Work. 13*th Photovoltaic Specialists Conference*, Washington DC, 5-8 June 1978, 1074-1079.

[14] Charles, J.P., Abdelkrim, M., Muoy, Y.H. and Mialhe, P. (1981) A Practical Method of Analysis of the Current-Voltage Characteristics of Solar Cells. *Solar Cells*, **4**, 169-178. https://doi.org/10.1016/0379-6787(81)90067-3

[15] Diantoro, M., Suprayogi, T., Hidayat, A., Taufiq, A., Fuad, A. and Suryana, R. (2018) Shockley's Equation Fit Analyses for Solar Cell Parameters from I-V Curves. *International Journal of Photoenergy*, **2018**, Article ID: 9214820. https://doi.org/10.1155/2018/9214820

[16] Saha, C., Agbu, N., Jinks, R. and Huda, M.N. (2018) Review Article of the Solar PV Parameters Estimation Using Evolutionary Algorithms. *MOJ Solar and Photoenergy Systems*, **2**, 66-78.

[17] Hachana, O., Hemsas, K.E., Tina, G.M. and Ventura, C. (2013) Comparison of Different Metaheuristic Algorithms for Parameter Identification of Photovoltaic Cell/Module. *Journal of Renewable and Sustainable Energy*, **5**, Article ID: 053122. https://doi.org/10.1063/1.4822054

[18] Tamrakar, R. and Gupta, A. (2015) A Review: Extraction of Solar Cell Modelling Parameters. *International Journal of Innovative Research in Electrical, Electronics, Instrumentation and Control Engineering*, **3**, 55-60. https://doi.org/10.17148/IJIREEICE.2015.3111

[19] Franco, R.A.P. and Vieira, F.H.T. (2018) Analytical Method for Extraction of the Single-Diode Model Parameters for Photovoltaic Panels from Datasheet Data. *Electronics Letters*, **54**, 519-521. https://doi.org/10.1049/el.2018.0402

[20] Abbassi, R., Abbassi, A., Jemli, M. and Chebbi, S. (2018) Identification of Unknown Parameters of Solar Cell Models: A Comprehensive Overview of Available Approaches. *Renewable and Sustainable Energy Reviews*, **90**, 453-474. https://doi.org/10.1016/j.rser.2018.03.011

[21] Ghani, F., Duke, M. and Carson, J. (2013) Numerical Calculation of Series and Shunt Resistances and Diode Quality Factor of a Photovoltaic Cell Using the Lambert W-Function. *Solar Energy*, **91**, 422-431. https://doi.org/10.1016/j.solener.2012.09.005

[22] Batzelis, E.I. and Papathanassiou, S.A. (2015) A Method for the Analytical Extraction of the Single-Diode PV Model Parameters. *IEEE Transactions on Sustainable Energy*, **7**, 504-512. https://doi.org/10.1109/TSTE.2015.2503435

[23] Ibrahim, H. and Anani, N. (2017) Evaluation of Analytical Methods for Parameter Extraction of PV Modules. *Energy Procedia*, **134**, 69-78. https://doi.org/10.1016/j.egypro.2017.09.601

[24] Mohapatra, A., Nayak, B. and Mohanty, K.B. (2017) Parameter Extraction of PV Module Using NLS Algorithm with Experimental Validation. *International Journal of Electrical and Computer Engineering*, **7**, 2392. https://doi.org/10.11591/ijece.v7i5.pp2392-2400

[25] Mahmoud, Y.A., Xiao, W. and Zeineldin, H.H. (2012) A Parameterization Approach for Enhancing PV Model Accuracy. *IEEE Transactions on Industrial Electronics*, **60**, 5708-5716. https://doi.org/10.1109/TIE.2012.2230606

[26] Huang, P.H. and Xiao, W., Peng, J.C.H. and Kirtley, J.L. (2015) Comprehensive Parameterization of Solar Cell: Improved Accuracy with Simulation Efficiency. *IEEE Transactions on Industrial Electronics*, **63**, 1549-1560. https://doi.org/10.1109/TIE.2015.2498139

[27] Sera, D., Teodorescu, R. and Rodriguez, P. (2007) PV Panel Model Based on Datasheet Values. 2007 *IEEE International Symposium on Industrial Electronics*, 4-7 June 2007, 2392-2396. https://doi.org/10.1109/ISIE.2007.4374981

[28] Yahfdhou, A., Mahmoud, A.K. and Youm, I. (2016) Evaluation and Determination of Seven and Five Parameters of a Photovoltaic Generator by an Iterative Method.

[29] Banwell, T.C. and Jayakumar, A. (2000) Exact Analytical Solution for Current Flow through Diode with Series Resistance. *Electronics Letters*, **36**, 291-292. https://doi.org/10.1049/el:20000301

[30] Li, Y., Huang, W., Huang, H., Hewitt, C., Chen, Y., Fang, G. and Carroll, D.L. (2013) Evaluation of Methods to Extract Parameters from Current-Voltage Characteristics of Solar Cells. *Solar Energy*, **90**, 51-57. https://doi.org/10.1016/j.solener.2012.12.005

[31] Zhang, Z.Z., Cheng, X.F. and Liu, J.L. (2013) An Improvement Method for Extracting Five Parameters of a Solar Cell Based on Lambert W-Function with the Current-Voltage Data. *In Applied Mechanics and Materials*, **291**, 38-42. https://doi.org/10.4028/www.scientific.net/AMM.291-294.38

[32] Cubas, J., Pindado, S. and De Manuel, C. (2014) Explicit Expressions for Solar Panel Equivalent Circuit Parameters Based on Analytical Formulation and the Lambert W-Function. *Energies*, **7**, 4098-4115. https://doi.org/10.3390/en7074098

[33] Nassar-Eddine, I., Obbadi, A., Errami, Y. and Agunaou, M. (2016) Parameter Estimation of Photovoltaic Modules Using Iterative Method and the Lambert W Function: A Comparative Study. *Energy Conversion and Management*, **119**, 37-48. https://doi.org/10.1016/j.enconman.2016.04.030

[34] Park, J.Y. and Choi, S.J. (2015) A Novel Datasheet-Based Parameter Extraction Method for a Single-Diode Photovoltaic Array Model. *Solar Energy*, **122**, 1235-1244. https://doi.org/10.1016/j.solener.2015.11.001

[35] Bonkoungou, D., Koalaga, Z., Njomo, D. and Zougmore, F. (2015) An Improved Numerical Approach for Photovoltaic Module Parameters Acquisition Based on Single-Diode Model. *International Journal of Current Engineering and Technology*, **5**, 3735-3742.

[36] Ayodele, T.R., Ogunjuyigbe, A.S.O. and Ekoh, E.E. (2016) Evaluation of Numerical Algorithms Used in Extracting the Parameters of a Single-Diode Photovoltaic Model. *Sustainable Energy Technologies and Assessments*, **13**, 51-59. https://doi.org/10.1016/j.seta.2015.11.003

[37] Shockley, W. (1949) The Theory of p-n Junctions in Semiconductors and p-n Junction Transistors. *Bell System Technical Journal*, **28**, 435-489. https://doi.org/10.1002/j.1538-7305.1949.tb03645.x

[38] Zaimi, M., El Achouby, H., Ibral, A. and Assaid, E.M. (2019) Determining Com-

bined Effects of Solar Radiation and Panel Junction Temperature on All Model-Parameters to Forecast Peak Power and Photovoltaic Yield of Solar Panel under Non-Standard Conditions. *Solar Energy*, **191**, 341-359. https://doi.org/10.1016/j.solener.2019.09.007

[39] Shen, W., Ding, Y., Choo, F.H., Wang, P., Loh, P.C. and Tan, K.K. (2009) Mathematical Model of a Solar Module for Energy Yield Simulation in Photovoltaic Systems. 2009 *International Conference on Power Electronics and Drive Systems*, Taipei, 2-5 November 2009, 336-341. https://doi.org/10.1109/PEDS.2009.5385657

[40] Hejri, M., Mokhtari, H., Azizian, M.R. and Söder, L. (2016) An Analytical-Numerical Approach for Parameter Determination of a Five-Parameter Single-Diode Model of Photovoltaic Cells and Modules. *International Journal of Sustainable Energy*, **35**, 396-410. https://doi.org/10.1080/14786451.2013.863886

[41] Atay, B.K. and Eminoğlu, U. (2019) A New Approach for Parameter Estimation of the Single-Diode Model for Photovoltaic Cells/Modules. *Turkish Journal of Electrical Engineering & Computer Sciences*, **27**, 3026-3039. https://doi.org/10.3906/elk-1805-161

[42] Rauschenbusch, H.S. (1971) Electrical Output of Shadowed Solar Arrays. *IEEE Transactions on Electron Devices*, **18**, 483-490. https://doi.org/10.1109/T-ED.1971.17231

[43] Castaner, L. and Silvestre, S. (2002) Modelling Photovoltaic Systems Using PSpice. John Wiley and Sons, Hoboken. https://doi.org/10.1002/0470855541

[44] Neville, R.C. (1995) Solar Energy Conversion: The Solar Cell. Elsevier, Amsterdam.

[45] Sze, S.M. and Ng, K.K. (2006) Physics of Semiconductor Devices. John Wiley and sons, Hoboken. https://doi.org/10.1002/0470068329

[46] Ataboev, O.K., Kabulov, R.R., Matchanov, N.A. and Egamov, S.R. (2019) Influence of Temperature on the Output Parameters of a Photovoltaic Module Based on Amorphous Hydrogenated Silicon. *Applied Solar Energy*, **55**, 159-167. https://doi.org/10.3103/S0003701X19030022

[47] Chenni, R., Makhlouf, M., Kerbache, T. and Bouzid, A. (2007) A Detailed Modeling Method for Photovoltaic Cells. *Energy*, **32**, 1724-1730. https://doi.org/10.1016/j.energy.2006.12.006

[48] Ndegwa, R., Simiyu, J., Ayieta, E. and Odero, N. (2020) A Fast and Accurate Analytical Method for Parameter Determination of a Photovoltaic System Based on Manufacturer's Data. *Journal of Renewable Energy*, **2020**, Article ID: 7580279. https://doi.org/10.1155/2020/7580279

[49] Phang, J.C.H., Chan, D.S.H. and Phillips, J.R. (1984) Accurate Analytical Method for the Extraction of Solar Cell Model Parameters. *Electronics Letters*, **20**, 406-408. https://doi.org/10.1049/el:19840281

[50] Cubas, J., Pindado, S. and Farrahi, A. (2013) New Method for Analytical Photovoltaic Parameter Extraction. 2013 *International Conference on Renewable Energy Research and Applications*, Madrid, 20-23 October 2013, 873-877. https://doi.org/10.1109/ICRERA.2013.6749874

[51] El Achouby, H., Zaimi, M., Ibral, A. and Assaid, E.M. (2018) New Analytical Approach for Modelling Effects of Temperature and Irradiance on Physical Parameters of Photovoltaic Solar Module. *Energy Conversion and Management*, **177**, 258-271. https://doi.org/10.1016/j.enconman.2018.09.054

[52] Villalva, M.G., Gazoli, J.R. and Ruppert Filho, E. (2009) Comprehensive Approach to Modeling and Simulation of Photovoltaic Arrays. *IEEE Transactions on Power Electronics*, **24**, 1198-1208. https://doi.org/10.1109/TPEL.2009.2013862

[53] Carrero, C., Rodriguez, J., Ramírez, D. and Platero, C. (2010) Simple Estimation of PV Modules Loss Resistances for Low Error Modelling. *Renewable Energy*, **35**, 1103-1108. https://doi.org/10.1016/j.renene.2009.10.025

[54] Reis, L.R.D., Camacho, J.R. and Novacki, D.F. (2017) The Newton Raphson Method in the Extraction of Parameters of PV Modules. *Proceedings of the International Conference on Renewable Energies and Power Quality*, Malaga, 4-6 April 2017, 634-639.

[55] Markvart, T., McEvoy, A. and Castaner, L. (2003) Practical Handbook of Photovoltaic: Fundamentals and Applications. Elsevier, Amsterdam.

[56] Schwingshackl, C., Petitta, M., Wagner, J.E., Belluardo, G., Moser, D., Castelli, M., Zebisch, M. and Tetzlaff, A. (2013) Wind Effect on PV Module Temperature: Analysis of Different Techniques for an Accurate Estimation. *Energy Procedia*, **40**, 77-86. https://doi.org/10.1016/j.egypro.2013.08.010